

Evaluation of a ^{125}I -labelled benzazepinone derived voltage-gated sodium channel blocker for imaging with SPECT†

Carlos Pérez-Medina,^a Niral Patel,^{a,b} Mathew Robson,^c Adam Badar,^b Mark F. Lythgoe^b and Erik Årstad^{*a}

Received 30th April 2012, Accepted 16th October 2012

DOI: 10.1039/c2ob26695d

Voltage-gated sodium channels (VGSCs) are a family of transmembrane proteins that mediate fast neurotransmission, and are integral to sustain physiological conditions and higher cognitive functions. Imaging of VGSCs *in vivo* holds promise as a tool to elucidate operational functions in the brain and to aid the treatment of a wide range of neurological diseases. To assess the suitability of 1-benzazepin-2-one derived VGSC blockers for imaging, we have prepared a ^{125}I -labelled analogue of BNZA and evaluated the tracer *in vivo*. In an automated patch-clamp assay, a diastereomeric mixture of the non-radioactive compound blocked the $\text{Na}_v1.2$ and $\text{Na}_v1.7$ VGSC isoforms with IC_{50} values of $4.1 \pm 1.5 \mu\text{M}$ and $0.25 \pm 0.07 \mu\text{M}$, respectively. [^3H]BTX displacement studies revealed a three-fold difference in affinity between the two diastereomers. Iodo-destannylation of a tin precursor with iodine-125 afforded the two diastereomerically pure tracers, which were used to assess binding to VGSCs *in vivo* by comparing their tissue distributions in mice. Whilst the results point to a lack of VGSC binding *in vivo*, SPECT imaging revealed highly localized uptake in the interscapular region, an area typically associated with brown adipose tissue, which in addition to high metabolic stability of the iodinated tracer, demonstrate the potential of 1-benzazepin-2-ones for *in vivo* imaging.

Introduction

Voltage-gated sodium channels (VGSCs) are a family of transmembrane proteins that initiate and propagate action potentials in electrically excitable cells.¹ Nine VGSC isoforms ($\text{Na}_v1.1$ – $\text{Na}_v1.9$) have been reported to date, each characterized by their distinct pharmacological and electrophysiological properties, as well as their unique expression patterns. $\text{Na}_v1.1$, $\text{Na}_v1.2$, $\text{Na}_v1.3$ and $\text{Na}_v1.6$ are mainly found in the central nervous system, whereas $\text{Na}_v1.4$ and $\text{Na}_v1.5$ are expressed in cardiac and skeletal muscle, and $\text{Na}_v1.7$, $\text{Na}_v1.8$ and $\text{Na}_v1.9$ are principally found in the peripheral nervous system.^{2,3} VGSCs are activated by membrane depolarisation which triggers a conformational change from the resting state to the open state, thereby allowing selective influx of sodium ions. The channels then undergo rapid

conformational change to the inactivated state before reverting back to their resting state.⁴

In addition to their role in mediating fast neurotransmission, VGSCs have been implicated in a number of pathological conditions including neuropathic pain, migraine, epilepsy, multiple sclerosis and neurodegeneration.^{5,6} Interestingly, up-regulation of VGSC expression has also been reported for several types of cancer,^{7,8} and is believed to enhance cellular migration and invasion.⁹ Radiotracers for imaging of VGSCs with positron emission tomography (PET) and single photon emission computed tomography (SPECT) therefore hold significant potential as tools to study activation of neuronal pathways, as well as for diagnostic imaging and treatment monitoring. Despite this potential, the field of VGSC imaging still remains largely unexplored.¹⁰

There are currently no established tracers for imaging of excitatory ion-channels *in vivo*. However, a number of tracers have been evaluated for imaging of *N*-methyl-*D*-aspartate receptors (NMDARs), and depending on their binding site, tracer distribution either reflects the activity or the expression pattern of the ion-channel.^{11–15} For VGSC tracers it is likely that both ion-channel expression and function can influence the binding pattern, at least for state-dependent ligands.⁴ In addition, the subtype selectivity of a tracer will dictate its potential applications. Yet, the high degree of homology between VGSC isoforms makes development of subtype selective ligands challenging, and at least for small molecules, the potency is

^aDepartment of Chemistry and Institute of Nuclear Medicine, UCL, 235 Euston Road (T-5), NW1 2BU London, United Kingdom.

E-mail: e.arstad@ucl.ac.uk; Fax: +44 (0)02076792344;

Tel: +44 (0)02076792344

^bCentre for Advanced Biomedical Imaging, Department of Medicine and UCL Institute of Child Health, 72 Huntley Street, WC1E 6DD London, United Kingdom

^cTumour Biology Section, UCL Cancer Institute, 72 Huntley Street, WC1E 6DD UCL London, United Kingdom

†Electronic supplementary information (ESI) available: Synthetic procedures, selected ^1H and ^{13}C NMR spectra and selected radio-HPLC chromatograms. See DOI: 10.1039/c2ob26695d

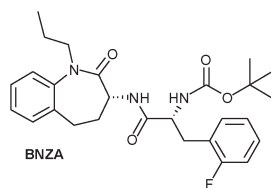


Fig. 1 Structure of BNZA.

often similar for many, if not all, of the Na_v isoforms.⁴ The binding of VGSC tracers *in vivo* is therefore likely to broadly reflect VGSC expression in the periphery as well as in the brain, with state-dependent ligands showing increased uptake in tissues with high electrical activity.

The 1-benzazepin-2-one derivative [³H]BNZA (Fig. 1) was recently reported to be a highly potent and state-dependent VGSC blocker that binds with low nanomolar affinity to rat brain synaptosomal membranes ($K_d = 1.53 \pm 0.46$ nM, $B_{max} = 3.4 \pm 1.2$ pmol mg⁻¹ of protein) as well as to transfected human hNa_v1.5 (K_d 0.97 nM) and hNa_v1.7 (K_d 1.6 nM) VGSC isoforms.¹⁶ Furthermore, analogues of BNZA have been shown to have good metabolic stability, and their anticonvulsant efficacy *in vivo* implies that derivatives of this compound class can penetrate the blood-brain barrier.¹⁷ Taken together, the results suggest that 1-benzazepin-2-ones meet many of the key criteria for tracer development, and that suitably radiolabelled derivatives of BNZA may enable imaging of VGSCs. To assess the suitability of 1-benzazepin-2-one derived VGSC blockers for imaging, we have prepared a ¹²⁵I-labelled analogue of BNZA and evaluated the tracer *in vivo*.

Materials and methods

Chemistry

All reagents were purchased from Sigma-Aldrich, except for 3-bromo-1,3,4,5-tetrahydro-benzo[*b*]azepin-2-one (**1**) which was purchased from Fluorochem, and were used without further purification. The synthetic procedures and analytical data for the compounds described herein can be found in the ESI.† Column chromatography was performed on silica-gel (VWR BDH-Pro-labo 40–63 μm). ¹H and ¹³C NMR spectra were recorded at room temperature on Bruker Avance 300 or 500 instruments operating at the frequency of 300 or 500 MHz for ¹H, and 75 or 125 MHz for ¹³C. All were internally referenced to the residual solvent peaks, CDCl₃ (7.26 ppm), DMSO-*d*₆ (2.49 ppm) or CD₃OD (3.31 ppm) for ¹H, CDCl₃ (δ 77.0 ppm), DMSO-*d*₆ (39.5 ppm) or CD₃OD (49.1 ppm) for ¹³C. High resolution mass data were recorded on a thermo Finnigan MAT900xp (CI/EI), a Waters LCT Premier XE (ES) or a VG70-SE (FAB) mass spectrometers. HPLC analysis was performed with an Agilent 1200 HPLC system equipped with a 1200 Series Diode Array Detector and Fluorescence Detector. The specific rotation ($[\alpha]_D^{20}$, $c = 1.0$, MeOH) of amine **3** was measured using a Perkin Elmer 241 polarimeter.

Radiochemistry

[¹²⁵I]NaI (>12.95 GBq mL⁻¹, 629 GBq mg⁻¹) was purchased from Perkin Elmer Life and Analytical Sciences (331 Treble

Cove Road, Billerica, MA 01862, USA) as a non-carrier-added solution in reductant free 10⁻⁵ M aqueous sodium hydroxide solution (pH 8–11).

Radio-HPLC

HPLC purification and analytical runs were carried out on a C18 Agilent Eclipse Plus column (4.6 × 150 mm, 5 μm) and monitored with a 254 UV detector and a Raytest Gabi NaI detector. The solvent systems used were water (0.1% TFA, solvent A) and methanol (0.1% TFA, solvent B) with a flow rate of 1 mL min⁻¹. Metabolite analysis was carried out on a C18 Agilent XDB column (4.6 × 150 mm, 5 μm) using water (0.1% formic acid, solvent A) and methanol (0.1% formic acid, solvent B) as solvent systems with a flow rate of 1 mL min⁻¹.

Log *D* determination

Log *D*_{7.4} of [¹²⁵I]h-9 was determined using the *n*-octanol shake flask method.¹⁸ Briefly, a solution of radioligand in *n*-octanol (500 μL, presaturated with PBS 7.4) was mixed with an equal volume of PBS 7.4 (presaturated with *n*-octanol) and shaken for 15 minutes at 900 rpm, after which time the mixture was centrifuged at 10 000 rpm for 5 minutes. The radioactivity present in both layers was measured in a gamma counter, and the *n*-octanol/PBS partition coefficient determined by dividing the radioactivity found in the *n*-octanol layer by that found in the PBS layer. The log value of this coefficient was then calculated. The process was repeated until a consistent value was obtained. The experiments were carried out in quadruplicate.

Animals

Female Balb/C mice were obtained from Charles River, UK. After arrival, the mice were allowed to acclimatise for at least 5 days in a room with constant temperature (21 °C) and humidity (30%). All efforts were made to reduce the number of animals used, and all experiments were conducted in accordance with the UK Animals (Scientific Procedures) Act, 1986 and the European Community Council Directive, 1986.

Metabolite analysis

Female Balb/C mice (6–10 weeks old and 15–20 g of weight) were injected with 2.4–3.4 MBq [¹²⁵I]h-9 in 120–300 μL saline solution (5% ethanol) *via* their lateral tail vein. The mice were anesthetized with isoflurane (5% mixed with medical air at a flow of 2 mL min⁻¹). At 5, 15, 30 and 60 min post injection blood was drawn out by cardiac puncture and, immediately afterwards, animals were sacrificed by cervical dislocation and brains removed. Blood was collected into heparinised tubes and centrifuged at 13 000 rpm for 1 min to separate plasma; 300 μL of plasma were mixed with 1200 μL of cold acetonitrile, vortexed and centrifuged at 13 000 rpm for 1 min. The supernatant was then transferred to a glass vial and mixed with 900 μL of water. Brain tissues were mixed with 1.5 mL acetonitrile–water 2 : 1 and homogenized, vortexed and centrifuged at 13 000 rpm for 1 min. The resulting supernatant was then mixed with 500 μL of

water and the resulting solution was centrifuged again as described above. Pellets and supernatants were separated and counted for radioactivity to determine recovery efficiency. An aliquot (1000 μL) of the supernatant obtained from the plasma and brain extracts was subjected to reversed-phase high-performance liquid chromatography (HPLC) analysis (Agilent C18 XDB column, $4.6 \times 150 \text{ mm}$, $5 \mu\text{m}$) using gradient elution from 50 to 90% solvent B over 15 minutes at a flow rate of 1 mL min^{-1} . The recovery from plasma was measured to be $93.4 \pm 1.0\%$ ($n = 3$) and from brain $80.8 \pm 0.1\%$ ($n = 3$). Sample workup was identical as described above. Results are expressed as percentages of the total activity \pm S.D.

Biodistribution studies

Biodistribution experiments were conducted on female Balb/C mice (6–10 weeks old and 15–20 g of weight). The radiotracer (0.2–0.4 MBq in 150–300 μL saline solution (5% ethanol)) was administered *via* the lateral tail vein. The mice were anesthetized with isoflurane (5%) mixed with medical air at a flow rate of 2 mL min^{-1} at predetermined time points after administration (5, 15, 30 and 60 min for [^{125}I]h-9 and 5 and 30 min for [^{125}I]l-9), blood was sampled through cardiac puncture, and the animals were then sacrificed by cervical dislocation. The radioactivity content in tissues of interest, (large and small intestine, stomach, kidneys, brain, bone (femur), liver, lungs, heart, skin, spleen, bladder, tail) was measured using a Wizard2 2470 Automatic Gamma Counter (Perkin Elmer). For each time point, 4 mice were used and the radioactivity uptake was calculated as the mean percentage injected dose per gram tissue \pm S.D.

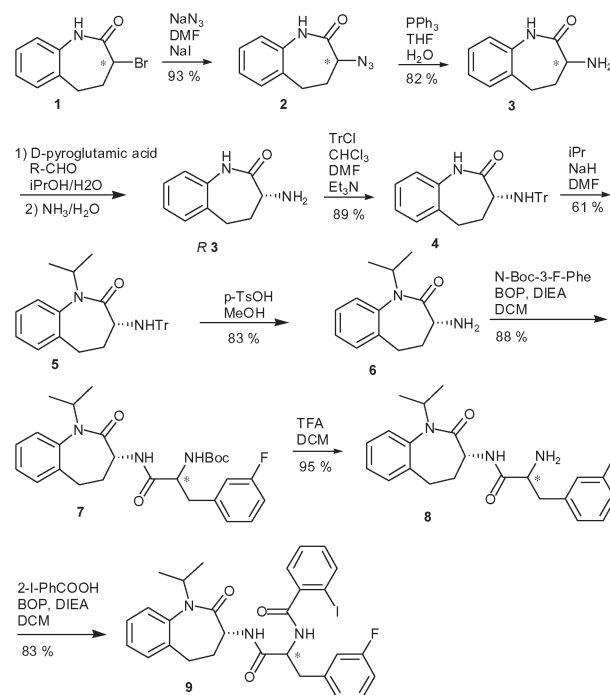
SPECT imaging

Female Balb/C mice (4–10 weeks old) were injected with 20–35 MBq [^{125}I]h-9 or [^{125}I]l-9 in 200–300 μL saline solution (5–7% ethanol, 0.1% TWEEN-80) *via* the lateral tail vein and then anesthetized with isoflurane mixed with medical air (5% for induction, 2% for maintenance). Animals were immediately placed in prone position on a heated bed ($37 \text{ }^\circ\text{C}$) under isoflurane anesthesia and scans were then performed using a NanoSPECT/CT small animal *in vivo* scanner (Bioscan Inc., 4590 MacArthur Blvd., NW, Washington D.C. 20007, USA). Whole body scans consisted of sixteen projections of varying duration and CT were recorded once the SPECT scans were finished. SPECT Images were reconstructed using HiSPECT software and *in vivo* Scope software was used for CT image reconstruction.

Results

Chemistry

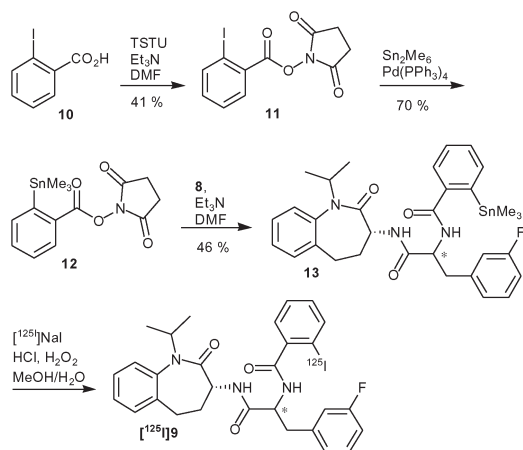
A nine step synthesis based on modified literature procedures¹⁹ was followed leading to the preparation of compound **9** in 9% overall yield (Scheme 1). Racemic 3-bromo-1,3,4,5-tetrahydrobenzo[*b*]azepin-2-one (**1**) was reacted with sodium azide in the presence of sodium iodide in DMF to afford azide **2**, which was subsequently converted *via* a Staudinger reaction to provide amine **3**.



Scheme 1 Synthesis of BNZA derivatives 7–9.

The racemic mixture of **3** was resolved by selective precipitation of the chiral *D*-pyroglutamate salt of the *R* enantiomer.²⁰ The recovery was 68% and the enantiomeric excess of the free amine **3** > 96%, as determined by polarimetry.²¹ Once isolated, the enantiomerically enriched amine **3** was tritylated to give **4**. Alkylation with isopropyl iodide in DMF provided the *N*-isopropyl lactam **5** in 61% yield. After deprotection of the trityl group with *p*-toluenesulfonic acid in methanol, the amine **6** was reacted with racemic *N*-Boc-DL-3-fluorophenylalanine using BOP as coupling agent to afford amide **7** in 88% yield. Removal of the Boc group with trifluoroacetic acid in dichloromethane provided the amine **8** in near quantitative yield. Finally, coupling of **8** with 2-iodobenzoic acid in the presence of BOP provided the non-radioactive reference compound **9** in 83% yield. Since racemic *N*-Boc-DL-3-fluorophenylalanine was used, compounds **7**, **8** and **9** were obtained as a mixture of diastereoisomers. Enriched fractions of both diastereoisomers of **9** were obtained by column chromatography, and excellent diastereomeric purity was achieved after separation by semi-preparative HPLC. The two diastereoisomers of **9** were termed *high*-9 (*h*-9), and *low*-9 (*l*-9) according to their relative affinities (see below). The absolute configuration around the α -carbon of the 3-fluorophenylalanine moiety was not determined for this study.

The tin precursor for radiolabelling with iodine-125 was prepared from amine **8** by reaction with the active ester **12**, which in turn was obtained from acid **10** after a two-step synthesis. 2-iodobenzoic acid (**10**) was treated with TSTU in DMF to produce the succinimidyl ester **11**, which upon reaction with hexamethylditin in the presence of palladium (0) furnished the stannated ester **12** in 70% yield. Subsequent reaction of **12** with amine **8** afforded the desired tin precursor **13** in a moderate 46% yield (Scheme 2).



Scheme 2 Synthesis of precursor **13** and radiolabelling of [^{125}I]**9**.

In vitro evaluation

The diastereomeric mixtures of compounds **7** and **9** were evaluated as VGSC blockers against the cloned human $\text{Na}_v1.2$ (h $\text{Na}_v1.2$, *SCN2A* gene) and $\text{Na}_v1.7$ (h $\text{Na}_v1.7$, *SCN9A* gene) isoforms expressed in CHO cells by means of automated patch-clamp as described elsewhere (ChanTest Corp., USA).²² The IC_{50} values for compound **9** were $4.1 \pm 1.5 \mu\text{M}$ and $0.25 \pm 0.07 \mu\text{M}$ for $\text{Na}_v1.2$ and $\text{Na}_v1.7$, respectively. For comparison, the IC_{50} values for compound **7** were $0.52 \pm 0.2 \mu\text{M}$ ($\text{Na}_v1.2$) and $0.13 \pm 0.02 \mu\text{M}$ ($\text{Na}_v1.7$). As an indirect way to measure the relative affinities of both diastereoisomers of **9**, a receptor [^3H]BTX binding assay (Ricerca Taiwan Ltd, Taiwan) was carried out.²³ Compound *h*-**9** displaced [^3H]BTX with an IC_{50} comparable to that of **7** (0.151 vs. $0.101 \mu\text{M}$), whereas *l*-**9** had three times lower affinity than its diastereoisomer ($\text{IC}_{50} = 0.484 \mu\text{M}$).

Radiochemistry

Treatment of the trimethyltin precursor **13** with [^{125}I]NaI in the presence of 0.1 M HCl and $1.4\% \text{ H}_2\text{O}_2$ for 30 min at 60°C provided [^{125}I]**9** in $24 \pm 4\%$ ($n = 11$) radiochemical yield with specific activity of $37.0 \pm 10.4 \text{ GBq } \mu\text{mol}^{-1}$ ($n = 8$) (Scheme 2). The two diastereomeric products of [^{125}I]**9**, *h*-**9** and *l*-**9**, were separated by radio-HPLC with excellent radiochemical (>99%) and diastereomeric (>99%) purities. The $\log D_{7,4}$ of [^{125}I]*h*-**9**

was measured to be 3.93 ± 0.01 ($n = 4$) using the *n*-octanol shake flask method.¹⁸

Biodistribution studies

The distribution of radioactivity was measured after *i.v.* injection of both diastereoisomers of [^{125}I]**9** in female Balb/C mice at pre-determined time points (5, 15, 30 and 60 minutes for [^{125}I]*h*-**9**, and 5 and 30 min for [^{125}I]*l*-**9**). Table 1 shows the uptake in selected tissues. Initially, a high uptake in the liver and kidneys was observed for [^{125}I]*h*-**9** with later time points dominated by high uptake in the intestines. The brain uptake was moderate ($0.92\% \text{ ID/g}$ for [^{125}I]*h*-**9** at 5 min post-injection) and gradually decreased over time. Blood clearance was slow, with $7.17 \pm 1.10\% \text{ ID/g}$ at 5 min post-injection and $3.25 \pm 0.45\% \text{ ID/g}$ at 60 min, resulting in poor brain-to-blood ratios values at all time points. The tissue distribution of [^{125}I]*l*-**9** was similar to that of [^{125}I]*h*-**9**, with high uptake in liver and kidneys at 5 min post-injection, and high uptake in the intestines at 30 min. The brain uptake was lower than that of [^{125}I]*h*-**9** at both time points investigated (0.68 vs. $0.92\% \text{ ID/g}$ at 5 min), and blood clearance was slightly faster, resulting in similar brain-to-blood ratios for both diastereoisomers.

Metabolite analysis

To assess the metabolic stability of [^{125}I]*h*-**9**, the composition of radioactive species in plasma and brain tissue was analyzed by radio-HPLC over a period of one hour after injection. [^{125}I]*h*-**9** was found to have excellent stability in both plasma and brain, and was the predominant radioactive species at all time points. In plasma, the fraction of the intact tracer [^{125}I]*h*-**9** was 93% at 5 min post-injection, 70% at 30 min, and 58% at 60 min ($n = 2$) (Fig. 2). Three metabolites were identified, all more polar than the parent compound. In the brain, the intact tracer [^{125}I]*h*-**9** was the only radioactive species found at the earlier times points (5, 10 and 15 min), with some minor metabolites (20% , $n = 2$) occurring 60 min after administration.

Imaging

Whole body SPECT/CT scans were recorded for both diastereoisomers of [^{125}I]**9** in female Balb/C mice. Overall, the SPECT

Table 1 Tissue distribution of [^{125}I]*h*-**9** and [^{125}I]*l*-**9** expressed as % ID/g \pm SD ($n \geq 3$)

	[^{125}I] <i>h</i> - 9				[^{125}I] <i>l</i> - 9	
	5 min	15 min	30 min	60 min	5 min	30 min
Blood	7.17 ± 1.10	4.66 ± 0.23	5.60 ± 0.21	3.25 ± 0.45	6.89 ± 0.81	4.05 ± 0.55
Heart	7.84 ± 1.20	4.27 ± 0.70	6.01 ± 0.81	2.96 ± 0.38	8.78 ± 1.84	4.27 ± 0.70
Liver	36.10 ± 2.1	27.50 ± 2.8	43.40 ± 3.4	18.80 ± 1.3	40.60 ± 3.5	31.70 ± 3.9
Kidneys	24.40 ± 1.0	12.80 ± 0.9	17.80 ± 1.7	7.34 ± 0.77	32.70 ± 2.9	20.30 ± 3.2
Brain	0.92 ± 0.08	0.49 ± 0.11	0.59 ± 0.07	0.26 ± 0.03	0.68 ± 0.10	0.34 ± 0.05
Lungs	7.98 ± 0.85	6.89 ± 0.93	6.28 ± 0.46	4.51 ± 0.68	9.10 ± 1.52	4.86 ± 0.69
Muscle	3.47 ± 0.18	2.53 ± 0.58	4.30 ± 1.3	1.71 ± 0.26	4.05 ± 0.56	2.41 ± 0.36
Spleen	10.10 ± 1.7	5.78 ± 0.61	6.94 ± 0.58	2.71 ± 0.23	10.10 ± 1.7	6.33 ± 0.83
Bone	2.11 ± 0.56	1.27 ± 0.36	1.76 ± 0.81	1.97 ± 0.76	5.09 ± 3.48	3.41 ± 1.33
Small Int.	9.89 ± 1.03	10.60 ± 1.8	39.50 ± 2.5	25.60 ± 2.7	9.63 ± 1.02	33.80 ± 8.2
Stom./L. Int.	4.42 ± 0.77	4.60 ± 1.0	10.20 ± 1.3	12.6 ± 2.4	6.39 ± 1.68	7.38 ± 1.7

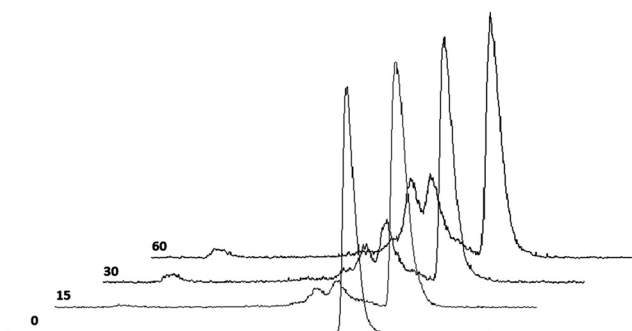


Fig. 2 HPLC radioactivity profiles of plasma samples at 0, 15, 30 and 60 min after injection of $[^{125}\text{I}]h\text{-9}$.

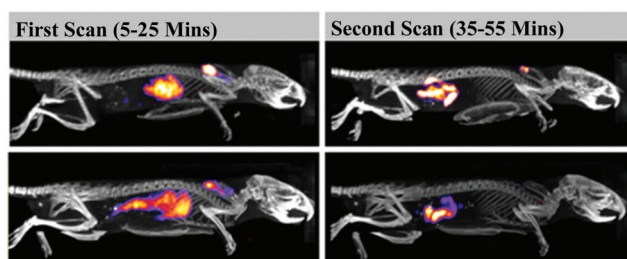


Fig. 3 SPECT/CT images showing the distribution of $[^{125}\text{I}]h\text{-9}$ (top) and $[^{125}\text{I}]l\text{-9}$ (bottom) in mice.

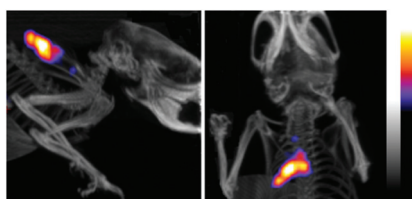


Fig. 4 Lateral (left) and anterior/posterior (right) SPECT/CT images of the uptake of $[^{125}\text{I}]h\text{-9}$ in the interscapular region at 55–65 min post-injection.

images (Fig. 3) were in good agreement with the biodistribution data, showing a high initial uptake of radioactivity in the liver (15–25 min post-injection). At the later time points (35–55 min post-injection) the images were dominated by high levels of activity in the intestines. Interestingly, in three out of a total of seven mice imaged with SPECT, a high uptake was observed in the interscapular region (Fig. 4). The uptake in this region appeared to be age related, as it was observed in adult mice (8–10 weeks old, $[^{125}\text{I}]h\text{-9}$ ($n = 2$) and $[^{125}\text{I}]l\text{-9}$ ($n = 1$)), but not in a group of younger animals (4–6 weeks, $[^{125}\text{I}]h\text{-9}$ ($n = 2$) and $[^{125}\text{I}]l\text{-9}$ ($n = 2$)). However, other factors may be involved, and further studies are required to determine the reason why the signal in the interscapular region was only observed in some, and not all, of the animals investigated. Unfortunately, the activity levels were too low to allow SPECT imaging of the regional distribution of $[^{125}\text{I}]h\text{-9}$ in the brain.

Discussion

We have prepared the novel radioiodinated 1-benzazepin-2-one $[^{125}\text{I}]h\text{-9}$ with the aim to evaluate the suitability of this compound class for imaging of VGSCs. Previously reported binding studies with $[^3\text{H}]$ BNZA using rat brain synaptosomal membranes suggest that radiolabelled 1-benzazepin-2-ones can be developed with sufficient affinity and binding potential for *in vivo* imaging.¹⁶ Our primary goal was therefore to assess the organ distribution and metabolic stability of $[^{125}\text{I}]h\text{-9}$ over a time frame relevant for imaging with PET and SPECT.

Iodine-125 was chosen for this study as it enables straightforward and reliable labelling by iodo-destannylation, and the long half-life (60 days) facilitates rapid biological evaluation. In addition, previously reported SAR studies with 1-benzazepin-2-ones revealed that benzamide derivatives bearing bulky lipophilic substituents in the 2-position, such as *tert*-butyl and trifluoromethyl, are well tolerated in the binding site.²⁴ As iodine is comparable in size and polarity, we envisaged that incorporation of a 2- $[^{125}\text{I}]$ iodobenzamide moiety as in $[^{125}\text{I}]h\text{-9}$ would allow labelling whilst retaining the biological activity of the lead compound **7**. However, the use of radioiodine for evaluation of small molecule tracers can be problematic as it results in high lipophilicity, a significant increase in molecular weight, and often poor metabolic stability. Despite these disadvantages, radioiodine has proven useful for evaluation of scaffolds as putative PET tracers, for instance to identify ligands with the required binding properties in biological tissues, and to assess biodistribution and metabolic stability.^{25,26}

The non-radioactive target compound **9** was prepared in 9% overall yield following a nine step synthesis. Coupling of the enantiomerically enriched amine **6** with racemic *N*-Boc-DL-3-fluorophenylalanine yielded a diastereomeric mixture of the previously reported VGSC blocker **7**. Deprotection of the BOC group and coupling of the resulting amine **8** with 2-iodobenzoic acid (**2**) provided the iodinated target compound **9**. Purification with semi-preparative HPLC allowed isolation of both diastereomers of **9** with excellent diastereomeric purity.

To assess the potency of **9** as a VGSC blocker the diastereomeric mixtures of **7** and **9** were evaluated in an automated patch-clamp assay (IWQ) against the human $\text{Na}_v1.2$ ($\text{hNa}_v1.2$, *SCN2A* gene) and $\text{Na}_v1.7$ ($\text{hNa}_v1.7$, *SCN9A* gene) isoforms expressed in CHO cells.²² Whereas the potency of **9** was largely retained against the $\text{Na}_v1.7$ isoform ($0.25 \pm 0.07 \mu\text{M}$ vs. $0.13 \pm 0.02 \mu\text{M}$ for **7**), the structural modifications were less well tolerated for $\text{Na}_v1.2$ ($4.1 \pm 1.5 \mu\text{M}$ vs. $0.52 \pm 0.2 \mu\text{M}$ for **7**). It is interesting to note that incorporation of the 2-iodobenzamide moiety increased the selectivity for $\text{hNa}_v1.7$ over $\text{Na}_v1.2$ from 4-fold for compound **7** to 16-fold for compound **9**. BNZA and the analogue **7** have previously been reported to be equipotent in a FRET assay with an IC_{50} of $0.03 \pm 0.02 \mu\text{M}$ against $\text{hNa}_v1.7$.¹⁶ The discrepancy between our results and the previously reported blocking efficiency for compound **7** is most likely due to the use of automated patch-clamp (IWQ) instead of FRET as the read-out, as well as the use of a diastereomeric mixture of **7** in this study. However, it should be noted that data obtained with IWQ can differ significantly from manual patch-clamp readings when using test compounds with high lipophilicity, and this may have affected the IC_{50} values obtained for **7** and **9**.²²

Since the VGSC blocker WIN17317-3 has been reported to displace both batrachotoxin ($[^3\text{H}]\text{BTX}$)²⁷ and $[^3\text{H}]\text{BNZA}$ ¹⁶ from their respective binding sites, we performed a $[^3\text{H}]\text{BTX}$ displacement study as an indirect way to measure the relative affinities of the two diastereoisomers of **9**. The diastereomer with the shortest retention on HPLC displaced $[^3\text{H}]\text{BTX}$ with an IC_{50} of 0.151 μM , whereas the IC_{50} of the slow eluting diastereomer was 0.484 μM . In comparison, the diastereomeric mixture of **7** was found to have an IC_{50} of 0.101 μM . The diastereomers of **9** were then termed high affinity **9**, *h*-**9**, and low affinity **9**, *l*-**9**, according to their relative affinities. Whilst the IC_{50} values for **7** and **9** are well above the low nanomolar affinity range typically required for *in vivo* imaging, the data cannot be directly related to binding affinities as the relationship with blocking potency and $[^3\text{H}]\text{BTX}$ displacement are complex.

The two radiolabelled diastereomers $[^{125}\text{I}]\text{h-9}$ and $[^{125}\text{I}]\text{l-9}$ were obtained in moderate radiochemical yield by treatment of the tin precursor **13** with $[^{125}\text{I}]\text{NaI}$ in the presence of hydrogen peroxide under acidic conditions. As lipophilicity affects brain uptake, metabolism and protein binding, we determined the $\log D_{7.4}$ of $[^{125}\text{I}]\text{h-9}$ using the *n*-octanol shake flask method. The high lipophilicity of $[^{125}\text{I}]\text{h-9}$ ($\log D_{7.4}$ of 3.93 ± 0.01) is a limitation with this study as it is likely to impair brain uptake, and result in low specific binding and high plasma protein binding *in vivo*.

In biodistribution studies, $[^{125}\text{I}]\text{h-9}$ and $[^{125}\text{I}]\text{l-9}$ behaved similarly, with the early time points dominated by uptake by the liver and kidneys. The brain uptake was moderate (0.92% ID/g 5 min post-injection) and gradually decreased over time. At later time points the majority of the activity was found in the intestines, consistent with hepatic clearance. There were no noteworthy differences in the tissue distributions of the two diastereomers of $[^{125}\text{I}]\text{9}$, and the lack of retention in the brain implies that no specific binding to VGSC channels was achieved. Surprisingly, whilst the SPECT images overall confirmed the results from the biodistribution studies, in the older animals (8–10 weeks) a high uptake was observed in the interscapular region in what appears to be a brown adipose tissue (BAT) depot. BAT has no known expression of VGSCs,²⁸ and the high uptake of $[^{125}\text{I}]\text{9}$ in the interscapular region is therefore most likely caused by a physiological effect, or potentially, cross activity with an unknown protein. Nevertheless, the highly localized uptake of $[^{125}\text{I}]\text{9}$ in the interscapular region demonstrates the potential of 1-benzazepin-2-ones for *in vivo* imaging, provided that sufficient VGSC binding affinity can be achieved. Whilst the brain uptake of $[^{125}\text{I}]\text{9}$ is moderate, it is likely that this at least in part is due to the high lipophilicity ($\log D_{7.4}$ 3.93 ± 0.01) and high molecular weight (MW 612.45) of **9**.

Conclusions

We have synthesized and radiolabelled a novel iodinated 1-benzazepin-2-one in order to evaluate the suitability of this compound class for imaging of VGSCs. The non-radioactive target compound was obtained as a pair of diastereomers. Iodo-destannylation of a tin precursor with iodine-125 afforded the diastereomerically pure tracers, which allowed us to assess binding to VGSCs *in vivo* by comparing their tissue distributions after

administration in mice. The distribution of both diastereomers was similar, and pointed to a lack of VGSC binding *in vivo*. However, a highly localized uptake in the interscapular region, and high metabolic stability of the iodinated tracer, demonstrate the potential of 1-benzazepin-2-ones for *in vivo* imaging. Further development of this compound class as VGSC tracers is therefore warranted, and we are currently investigating strategies for labelling 1-benzazepin-2-ones with fluorine-18.

Acknowledgements

This work was undertaken at UCLH/UCL who received a proportion of funding from the Department of Health's NIHR Biomedical Research Centres funding scheme (E. Årstad and C. Pérez-Medina). We also acknowledge support from the Medical Research Council (N. Patel) and King's College London and UCL Comprehensive Cancer Imaging Centre CR-UK & EPSRC, in association with the MRC and DoH (England) (M.F. Lythgoe).

Notes and references

- W. A. Catterall, *Neuron*, 2000, **26**, 13–25.
- F. H. Yu and W. A. Catterall, *Genome Biology*, 2003, **4**, 207.
- A. L. Goldin, *Annu. Rev. Physiol.*, 2001, **63**, 871–894.
- T. Anger, D. J. Madge, M. Mulla and D. Riddall, *J. Med. Chem.*, 2001, **44**, 115–137.
- M. Mantegazza, G. Curia, G. Biagini, D. S. Ragsdale and M. Avoli, *Lancet Neurol.*, 2010, **9**, 413–424.
- S. D. Dib-Hajj, T. R. Cummins, J. A. Black and S. G. Waxman, *Annu. Rev. Neurosci.*, 2010, **33**, 325–347.
- J. K. Diss, S. N. Archer, J. Hirano, S. P. Fraser and M. B. Djamgoz, *Prostate*, 2001, **48**, 165–178.
- D. Diaz, D. M. Delgadillo, E. Hernandez-Gallegos, M. E. Ramirez-Dominguez, L. M. Hinojosa, C. S. Ortiz, J. Berumen, J. Camacho and J. C. Gomora, *J. Cell. Physiol.*, 2007, **210**, 469–478.
- W. J. Brackenbury, M. B. Djamgoz and L. L. Isom, *Neuroscientist*, 2008, **14**, 571–583.
- No papers have yet been published on tracers for imaging of VGSCs, however, a patent has been filed (Årstad, E. US2010247435 (A1), 2007) and we and others have published conference abstracts: C. Pérez-Medina, *et al.*, *J. Label. Compd. Radiopharm.*, 2011, **54**(S1), S287–S288; A. Hoehne, *et al.*, *J. Labelled Compd. Radiopharm.*, 2011, **54**, S1–S2.
- J. Owens, A. A. Tebbutt, A. L. McGregor, K. Kodama, S. S. Magar, M. E. Perlman, D. J. Robins, G. J. Durant and J. McCulloch, *Nucl. Med. Biol.*, 2000, **27**, 557–564.
- J. M. Stone, K. Erlandsson, E. Årstad, R. A. Bressan, L. Squassante, V. Teneggi, P. J. Ell and L. S. Pilowsky, *Nucl. Med. Biol.*, 2006, **33**, 239–243.
- R. J. J. Knol, K. De Bruin, B. L. F. Van Eck-smit, S. Pimlott, D. J. Wyper and J. Booij, *Synapse*, 2009, **63**, 557.
- E. G. Robins, Y. J. Zhao, I. Khan, A. Wilson, S. K. Luthra and E. Årstad, *Bioorg. Med. Chem. Lett.*, 2010, **20**(5), 1749–1751.
- F. Sobrio, G. Gilbert, C. Perrio, L. Barré and D. Debruyne, *Mini Rev. Med. Chem.*, 2010, **10**(9), 870–886.
- B. S. Williams, J. P. Felix, B. T. Priest, R. M. Brochu, K. Dai, S. B. Hoyt, C. London, Y. S. Tang, J. L. Duffy, W. H. Parsons, G. J. Kaczorowski and M. L. Garcia, *Biochemistry*, 2007, **46**, 14693–14703.
- S. B. Hoyt, C. London, M. J. Wyratt, M. H. Fisher, D. E. Cashen, J. P. Felix, M. L. Garcia, X. Li, K. A. Lyons, M. D. Euan, W. J. Martin, B. T. Priest, M. M. Smith, V. A. Warren, B. S. Williams, G. J. Kaczorowski and W. H. Parsons, *Bioorg. Med. Chem. Lett.*, 2008, **18**, 1963–1966.
- E. Årstad, S. Platzer, A. Berthele, L. S. Pilowsky, S. K. Luthra, H. J. Wester and G. Henriksen, *Bioorg. Med. Chem.*, 2006, **14**, 6307–6313.
- S. B. Hoyt, C. London, D. Gorin, M. J. Wyratt, M. H. Fisher, C. Abbadié, J. P. Felix, M. L. Garcia, X. Li, K. A. Lyons, E. McGowan,

- D. E. Macintyre, W. J. Martin, B. T. Priest, A. Ritter, M. M. Smith, V. A. Warren, B. S. Williams, G. J. Kaczorowski and W. H. Parsons, *Bioorg. Med. Chem. Lett.*, 2007, **17**, 4630–4634.
- 20 J. D. Armstrong III, K. K. Eng, J. L. Keller, R. M. Purick, F. W. Hartner Jr., W. Choi, D. Askin and R. P. Volante, *Tetrahedron Lett.*, 1994, **35**, 3239–3242.
- 21 W. R. Schoen, J. M. Pisano, K. Prendergast, M. J. Wyvratt Jr., M. H. Fisher, K. Cheng, W. W. Chan, B. Butler, R. G. Smith and R. G. Ball, *J. Med. Chem.*, 1994, **37**, 897–906.
- 22 B. A. Wible, Y. A. Kuryshv, S. S. Smith, Z. Liu and A. M. Brown, *Assay Drug Dev. Technol.*, 2008, **6**, 765–780.
- 23 W. A. Catterall, C. S. Morrow, J. W. Daly and G. B. Brown, *J. Biol. Chem.*, 1981, **256**, 8922–8927.
- 24 S. B. Hoyt, C. London, H. Ok, E. Gonzalez, J. L. Duffy, C. Abbadie, B. Dean, J. P. Felix and M. L. Garcia, *et al.*, *Bioorg. Med. Chem. Lett.*, 2007, **17**, 6172–6177.
- 25 Z. P. Zhuang, M. P. Kung, C. Hou, D. M. Skovronsky, T. L. Gur, K. Plössl, J. Q. Trojanowski, V. M. Y. Lee and H. F. Kung, *J. Med. Chem.*, 2001, **44**, 1905–1914.
- 26 G. Smith, M. Glaser, M. Perumal, Q. D. Nguyen, B. Shan, E. Årstad and E. O. Aboagye, *J. Med. Chem.*, 2008, **51**(24), 8057–8067.
- 27 S. G. Wanner, H. Glossmann, H. G. Knaus, R. Baker, W. Parsons, K. M. Rupprecht, R. Brochu, C. J. Cohen, W. Schmalhofer, M. Smith, V. Warren, M. L. Garcia and G. J. Kaczorowski, *Biochemistry*, 1999, **38**, 11137–11146.
- 28 B. Cannon and J. Nedergaard, *Physiol. Rev.*, 2004, **84**, 277–359.